Inelasticity increases the critical strain for the onset of creases on hydrogels

Jiawei Yang, Widusha Illeperuma, Zhigang Suo [*]

John A. Paulson School of Engineering and Applied Sciences, Kavli Institute for Nanobio Science and Technology, Harvard University, Cambridge, MA 02138, USA

ABSTRACT

When a soft material (gel, elastomer, or biological tissue) is compressed beyond a critical strain, its smooth surface forms creases. During this process, a material particle near a crease undergoes a path of load and unload. If the material is elastic, the load and unload do not dissipate energy, and the crease sets in at a critical strain about 0.35. If the material is inelastic, however, the load and unload dissipate energy, and the crease is expected to set in at a higher critical strain. Here we study the effect of inelasticity on the onset of creases using alginate-polyacrylamide hydrogels. Such a hydrogel consists of two interpenetrating polymer networks: a polyacrylamide network of covalent crosslinks, and an alginate network of ionic crosslinks. The former is stretchy and elastic, while the latter unzips at a small stretch and causes inelasticity. We prepare alginate-polyacrylamide hydrogels with various degrees of inelasticity by varying the concentration of alginate. Our experiment confirms that larger degree of inelasticity leads to larger critical strain for crease. This study shows an example that the chemistry of materials affects the mechanics of creases.

© 2020 Elsevier Ltd. All rights reserved.

1. Introduction

A crease is a localized self-contact that forms on the surface of a soft material under compression [1,2]. During the formation of a crease, the material particles around the crease experience load and unload. Inelasticity dissipates energy and is expected to retard the critical strain for the onset of crease. For the time being, consider load and unload of a material under uniaxial stress. When the material is elastic, the load and unload follow the same stress–strain curve, and dissipate no energy (Fig. 1(a)). When the material is inelastic, the load and unload follow different stress–strain curves, and the area enclosed by the two curves is the dissipated energy per unit volume of the material (Fig. 1(b)).

For an elastic material, the critical strain for the onset of crease is around 0.35 [3,4]. Such creases are observed widely [5], on an elastomer or hydrogel under bending or compression [3,4,6–8], on a hydrogel swelling under constraint [9–14], on a tissue growing under constraint [15–18], and on a hydrogel or a dielectric elastomer under electric fields [19–22]. Furthermore, creases have been harnessed to achieve functions, including a mechanically gated electrical switch [23], an adaptive lens [24], as well as surfaces capable of controlling wettability [25], chemical patterns [26], enzymatic activity [27] and cellular behavior [11]. For

an inelastic material, energy dissipation can retard the formation of creases [28]. For example, creases can form on a high-density polyethylene (HDPE) at a strain of 0.49 [28], in a compressed plastic film on a compliant substrate [29] and under electric fields [30], but cannot form on metals (aluminum, copper, and stainless steel) [28].

Here we study the effect of inelasticity on creases using a family of hydrogels, which we can prepare to exhibit various degrees of inelasticity. A hydrogel contains a three-dimensional polymer network, which offers means to tune the mechanical properties by changing proportions of the chemicals in the precursor. For example, the elastic modulus increases with the crosslinking density [31], and the toughness improves by incorporating sacrificial bonds [32] (e.g., weak bonds [33,34], polymer chains [35], clays [36], brittle polymer networks [37,38], and fibers [39]). Importantly, the hysteresis of the hydrogel can be also tuned by these sacrificial bonds.

For this study, we prepare a series of alginate-polyacrylamide (alg-PAAM) hydrogels, which we developed before [38]. The alg-PAAM hydrogel consists of two interpenetrating polymer networks: a polyacrylamide (PAAM) network of covalent crosslinks, and an alginate network of ionic crosslinks (Fig. 2(a)). The PAAM network is stretchy while the alginate network is brittle. When the alg-PAAM hydrogel is deformed, the PAAM network is elastic and remains intact, but the alginate network breaks by unzipping the ionic bonds (Fig. 2(b)). The network breaking process is inelastic, which causes hysteresis and dissipates energy. To tune

[*] Corresponding author.
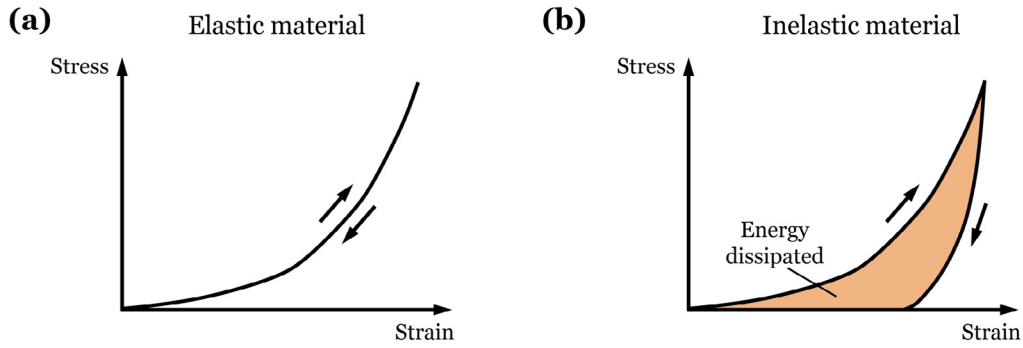*E-mail address:* suo@seas.harvard.edu (Z. Suo).

Fig. 1. Load and unload stress–strain curves in elastic and inelastic materials. (a) For an elastic material, load and unload follow the same stress–strain curve, and no energy is dissipated. (b) For an inelastic material, load and unload follow different stress–strain curves. The Area between the two curves is the energy dissipated per unit volume of the material.
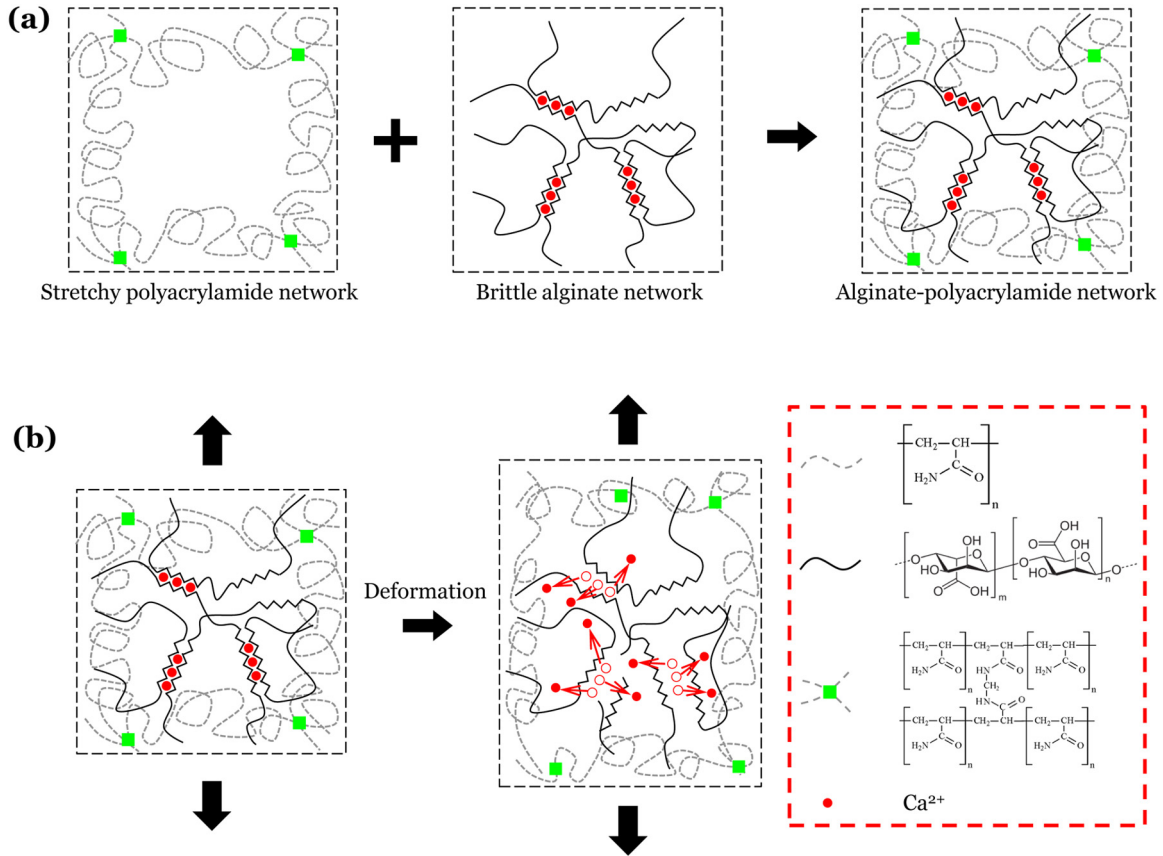

Fig. 2. Alginate-polyacrylamide hydrogel. (a) A alginate-polyacrylamide network consists of a stretchy polyacrylamide network and a brittle alginate network. (b) When the alginate-polyacrylamide network is deformed, the polyacrylamide network is elastic and remains intact, but the brittle alginate network breaks by unzipping the ionic bonds.

the amount of hysteresis of the hydrogel, we vary the alginate concentration while keep the calcium concentration relative to alginate fixed. As the alginate concentration increases, more ionic bonds participate in forming alginate network, and also more ionic bonds are ruptured in the deformation, leading to larger hysteresis. We prepare several alg-PAAM hydrogels of disk shape with different alginate concentration. The stress–strain curve of each hydrogel specimen is measured to show the size of hysteresis with different alginate concentration. We next perform compression tests for each hydrogel specimen and measure the critical strains for the onset of creases. We discuss these experimental findings in terms of the mechanics of creases and the chemistry of the hydrogels.

2. Experimental methods

2.1. Synthesis of alg-PAAM hydrogel

We synthesize alg-PAAM hydrogels using a two-step method described before [40] (Fig. 3). In the first step, we prepared PAAM hydrogels with uncrosslinked alginate chains. We first mixed 40.56 g acrylamide powder (AAM, Sigma-Aldrich, A8887) and sodium alginate powder (FMC Biopolymer, Manugel GMB) of weights 0 g, 1.13 g, 3 g and 6.78 g (alginate/AAM = 0, 2.78 wt%, 7.4 wt% and 16.72 wt%) in 300 ml deionized water. We added N,N'-methylenebisacrylamide (MBAA; Sigma-Aldrich, M7279) as covalent crosslinker (MBAA to acrylamide weight ratio is 0.0006:1), N,N,N',N'-tetramethylethylenediamine (TEMED;
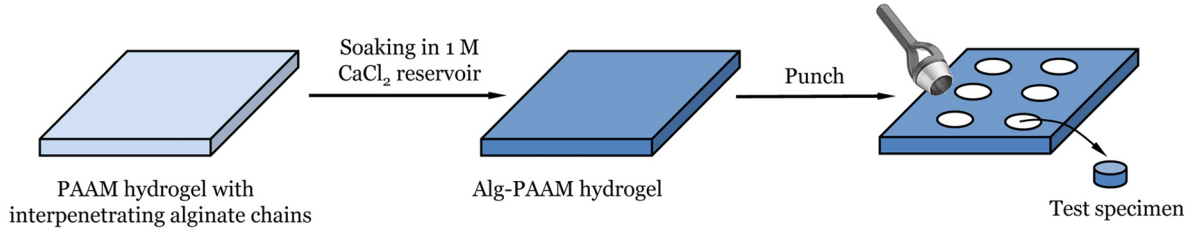
Fig. 3. Preparation of alg-PAAM hydrogel specimens. The synthesized PAAM hydrogel with different alginate concentration is soaked in a 1 M CaCl₂ reservoir to allow calcium ions to diffuse into the hydrogel and ionically crosslink alginate chains to a alginate network, which leads to a alg-PAAM network. A test specimen of disk shape is obtained by punching the alg-PAAM hydrogel.
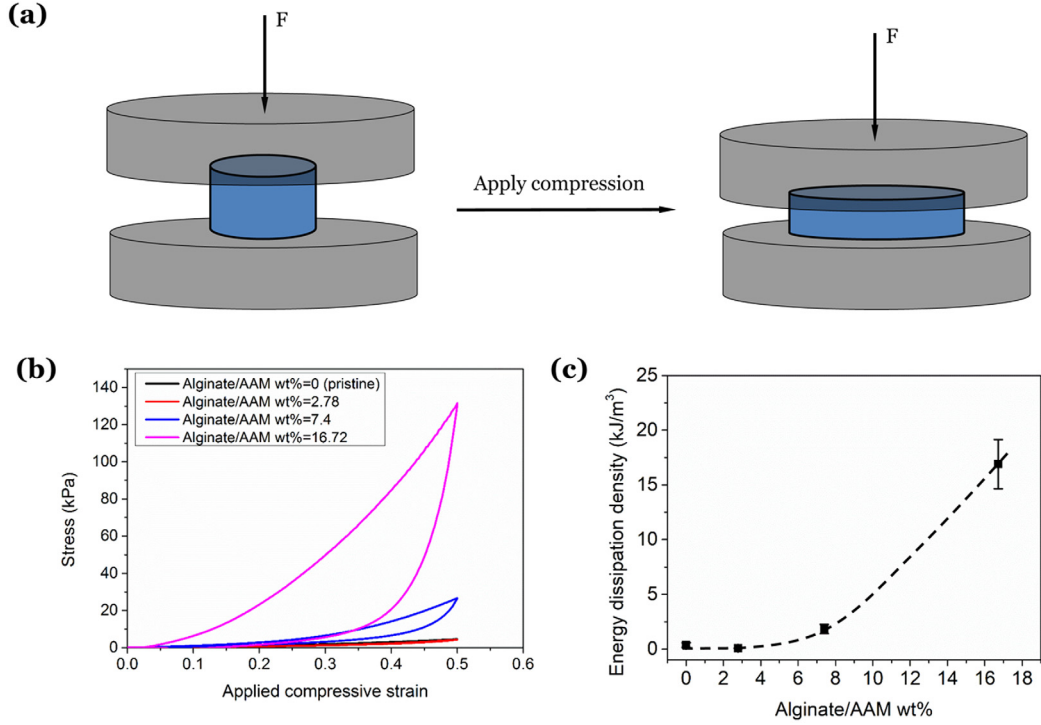

Fig. 4. Load–unload behaviors of alginate-polyacrylamide hydrogels. (a) Schematic illustrations of the compression tests to measure the load–unload curves. The compression is applied in the specimen's thickness direction. (b) Load and unload curves of alg-PAAM hydrogels with different alginate concentration. (c) Density of energy dissipation increases with the alginate concentration.

Sigma-Aldrich, T7024) as crosslinking accelerator (TEMED to acrylamide weight ratio is 0.0028:1), and ammonium persulfate (APS; Sigma-Aldrich, A9164) as initiator (APS to acrylamide weight ratio is 0.01:1) into the precursor solutions. The precursor solutions were sufficiently mixed and then poured into square glass molds of dimensions 60 mm × 60 mm × 6 mm, and covered with a 3-mm-thick glass plate. The precursor solutions were stored at room temperature overnight to complete polymerization. Afterwards, we took the hydrogel out to proceed next step.

In the second step, except for the pure PAAM hydrogel (alginate/AAM = 0 wt%) which was directly used in the compression test, the rest PAAM hydrogels with different alginate concentration were soaked in a 1 M calcium chloride (Sigma-Aldrich, 793639) solution for at least 5 days. The soaking process allowed calcium ions to diffuse into the hydrogels and ionically crosslink the alginate chains to alginate networks. Thus, the PAAM hydrogels with alginate chains became alg-PAAM hydrogels.

The alg-PAAM hydrogels were then punched into a disk shape of 15 mm in diameter and 6 mm in thickness (Hammer-Driven Hole Punches; McMaster-Carr). The disk shape hydrogel was a test specimen.

2.2. Stress–strain curves of alg-PAAM hydrogels

The stress–strain curves of alg-PAAM hydrogels with different alginate concentrations were measured through compression tests on an Instron test machine (model 3342). All tests were performed in air, at room temperature, using a 500-N load cell. Before tests, Teflon films of thickness ∼0.254 mm (Extreme-Temperature Slippery PTFE; McMaster-Carr) were pre-attached on both compression platens to lower the friction between the hydrogel and the platen. An aerosol lubricant (WD-40) was then sprayed on the Teflon films to further reduce friction. We placed alg-PAAM hydrogel between two platens, and applied compression in the specimen's thickness direction (Fig. 4(a)). The displacement rate was fixed at 10 mm/min. The compressive strain (applied displacement divided by the thickness of the hydrogel) was applied up to 50% of the initial thickness, and then unloaded. The load and unload curves were recorded.

2.3. Crease tests for alg-PAAM hydrogels

The crease tests for alg-PAAM hydrogels were performed under the same experiment setups as described above, but with
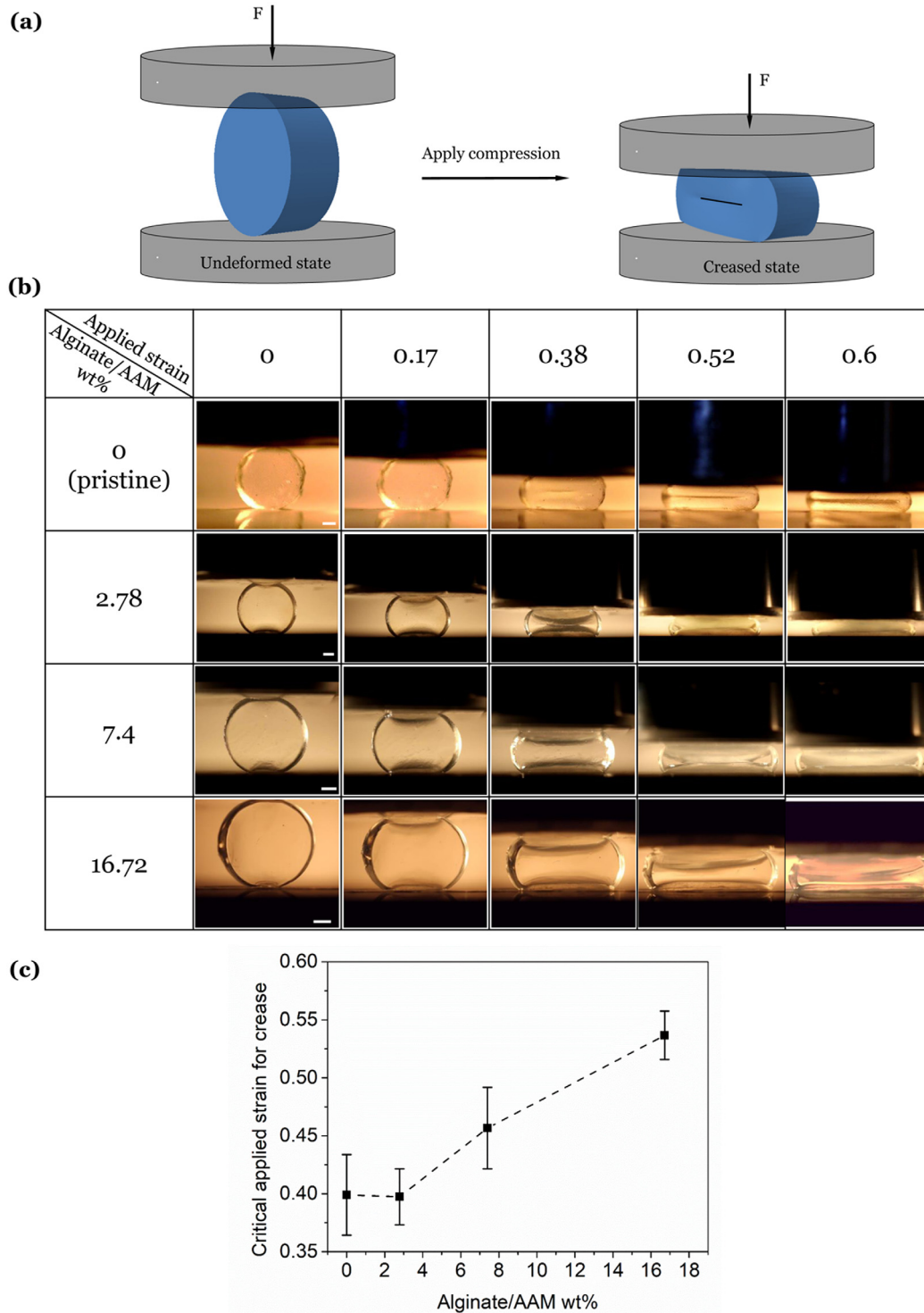
Fig. 5. Crease tests. (a) Schematic illustrations of the compression tests to trigger creases. The compression is applied along the specimen's diameter direction. (b) A sequence of snapshots of alg-PAAM hydrogels with different alginate concentration at varied applied strain. Creases are observed first in the specimens with alginate/AAM = 0 wt% and 2.78 wt%, and then 7.4 wt% and finally 16.72 wt%. The scale bar is 2 mm. (c) Critical applied strains of creases increase with the alginate concentration.

the compression direction being in the specimen's diameter direction (Fig. 5(a)). The compression generated an inhomogeneous strain field in the specimen, with the highest strain at the center (Fig. 6(a)). Such strain concentration was leveraged to trigger creases at a relatively lower applied strain. Therefore, creases were expected to form at the center of both sides of the specimen. The displacement rate was fixed at 10 mm/min. The entire crease tests were recorded by a digital camera, and the critical applied strains were determined from video.

3. Results and discussion

The load and unload curves of alg-PAAM hydrogels with different alginate concentrations vary distinctively (Fig. 4(b)). When
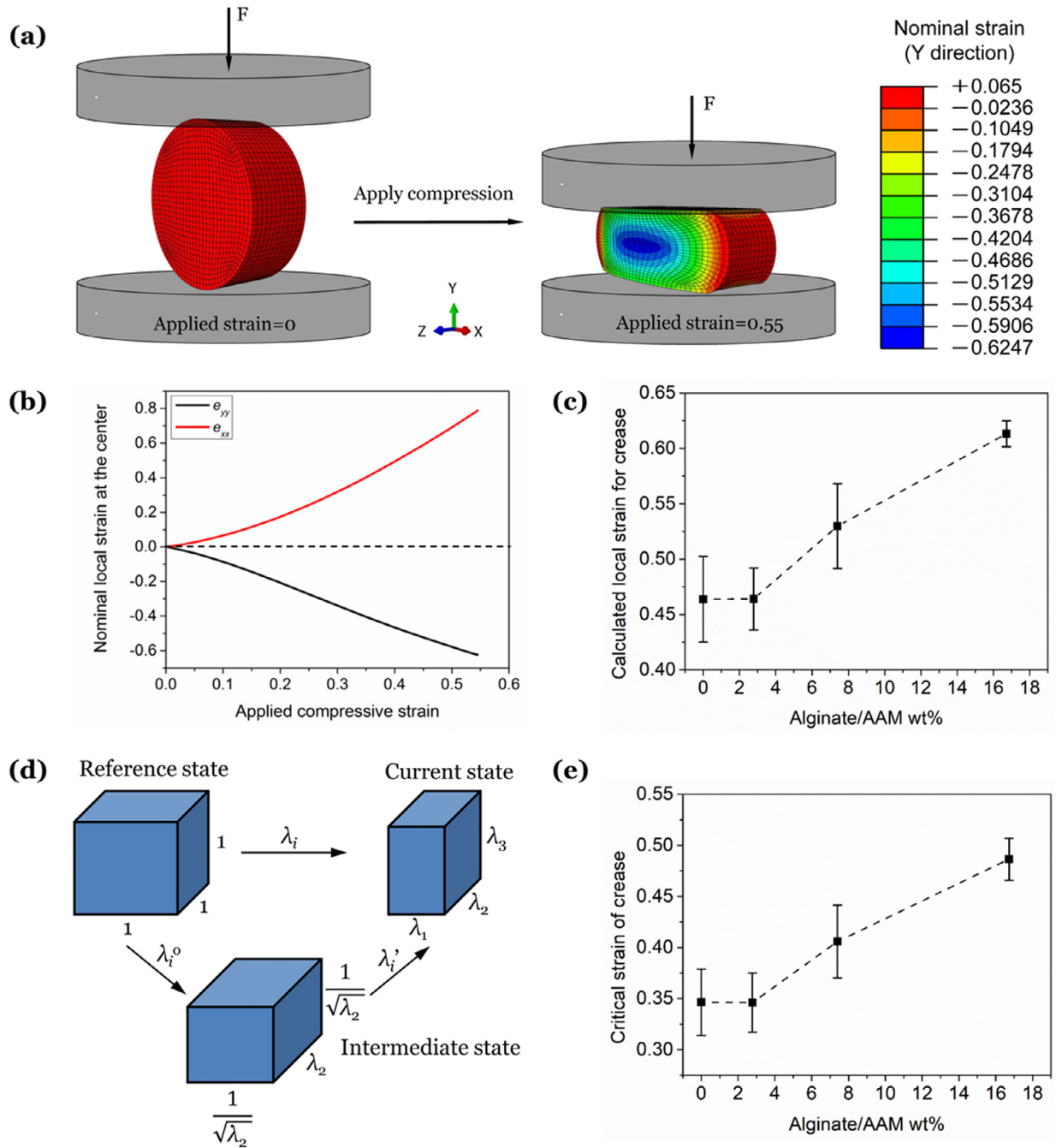
Fig. 6. Critical strains in plane strain condition. (a) The strain field in the specimen along the loading direction. Higher strain is observed at the center of the specimen. Images are generated from finite element simulation. (b) The local strains e_{yy} and e_{xx} at the center of the specimen evolve with applied strain. (c) The local critical strains for creases increase with alginate concentration. (d) A schematic illustration to convert strains in generalized plane-strain condition to those in plane-strain condition. (e) Critical strains in plane strain condition increase with alginate concentration.

the alginate concentration is low, e.g., alginate/acrylamide = 2.78 wt%, the load and unload curve is almost the same as that for the specimen without hysteresis (alginate/acrylamide = 0 wt%). The hysteresis is negligible. As alginate concentration increases, e.g., alginate/acrylamide = 16.72 wt%, the alg-PAAM hydrogel stiffens. The stress level increases by two orders of magnitude, from 5 kPa to 130 kPa, at the strain of 0.5. Upon unloading, the unloading path differs from the loading path, leading to a substantial hysteresis and a large residual strain. The dissipated energy during load–unload increases with alginate concentration (Fig. 4(c)). When alginate/acrylamide = 2.78 wt%, the energy dissipated is 0.05 kJ/m³, almost same with that of a PAAM hydrogel,

indicating that a small amount of ionic bonds breaks and little energy is dissipated. As alginate concentration increases to 16.72 wt%, the energy dissipation raises drastically to 15.33 kJ/m³. This large dissipation is due to the unzip of a large number of ionic bonds in the alginate network.

To investigate the effect of hysteresis on the formation of creases, we use the same types of specimens but apply compression in the diameter direction. We record the critical strain to initiate the creases (Fig. 5(a)). Unlike the compression in the thickness direction, where the deformation is homogeneous, compression in the diameter direction generates an inhomogeneous strain field, and the largest strain occurs in the center of the specimen

(Fig. 6(a)). A sequence of deformation of alg-PAAM hydrogels with different alginate concentration is captured at different applied strain (Fig. 5(b)). Before tests (applied strain = 0), the surfaces of all specimens are smooth. As the applied strain increases to 0.17, the surfaces of all specimens remain smooth. At applied strain of 0.38, we observe that the specimens with alginate/AAM = 0 wt% and 2.78 wt% start to form crease at the center of the specimen on both sides, while the surfaces of the other two specimens are still smooth. When the applied strain further increases to 0.52, the two already formed creases extend across the surface. The specimen with alginate/acrylamide = 7.4 wt% starts to form creases. At applied strain as large as 0.6, creases finally form in the specimen with alginate/acrylamide = 16.72 wt%. The experimental observations clearly show that the formation of crease retards as the hysteresis of alg-PAAM hydrogel increases (Fig. 5(c)). The mechanism can be understood as follows. In order to form a crease, a material particle on the flat surface serving as a crease nucleation point needs to move downwards into the material and subsequently causes deformation nearby. Each material particle around the crease tip undergoes non-proportional loading. For example, consider the material particle directly beneath the crease tip. In the direction of the applied load, the material particle is subject to a compressive strain prior to the formation of the crease, but is subject to a tensile strain after the formation of the crease. Inelastic deformation (e.g., plastic flow, material damage) dissipates energy. As a result, hydrogels of larger hysteresis dissipate more energy and store less elastic energy. To gain sufficient elastic energy to initiate the crease, the applied compressive strain must increase, thus leading to a larger critical strain for the onset of crease.

We next carry out finite element simulations (Abaqus 6.12/standard) to calculate the local strain at the center of the specimen. Note that the finite element calculation here does not attempt to simulate the formation of crease. In a previous study, we carried out a finite element calculation to determine the critical strains for the onset of creases in elastic–plastic materials [28]. The intention here is to determine the strain at the center of a disk prior to the formation of creases. We build a computational model of the same geometry of the specimen and mesh with 8-node linear brick C3D8RH. The specimen is modeled as the neo-Hooken material (the type of model does not affect the strain field). Due to symmetry, only 1/8 of model is simulated. We choose front-right part of the model and assign the left plane, the bottom plane and the back plane as symmetric planes. An analytic rigid plane functioning as the compression platen is placed in contact with the disk on the top. The contact interface is assumed frictionless, since we do not observe obvious deformation constraint at the hydrogel boundaries in the experiments. A compressive strain is applied vertically on the rigid plane, and the vertical strain field of the specimen is determined (Fig. 6(a)). The maximum strain takes place in the center of the disk. The local strains e_{xx} and e_{yy} at the center of the specimen are calculated as a function of applied strain (Fig. 6(b)), and show a moderate strain concentration. Using the experimentally measured critical strains for creases (Fig. 5(c)), we calculate the corresponding local critical strains e_{yy} at the center (Fig. 6(c)).

We further convert the local critical strains into those in standard plane strain condition. As the specimen deforms, the strain in its perpendicular direction e_{xx} at the center of the specimen is finite. That is, the formation of crease is in a state of generalized plane strain condition, which can be transformed into an equivalent plane strain condition following the procedure described in ref. [4] (Fig. 6(d)) (the material can be regarded as a nonlinear, incompressible elastic material before creases set in since there is no unload taking place). Briefly, a unit cube in the reference state deforms to a current state where crease forms by principal

stretches λ_i ($i = 1, 2, 3$); imagine an intermediate state, where the unit cube is first stretched by $\lambda_2^0 = \lambda_2$, with $\lambda_1^0 = \lambda_3^0 = 1/\sqrt{\lambda_2}$. This intermediate state can be regarded as a new reference state; let λ_i' be the stretches measured from the intermediate state to the current state. λ_2 is fixed in the deformation, $\lambda_2' = 1$, and λ_1' is the critical stretch in plane strain condition. We have the following relations

$$\lambda_1 = \lambda_1'/\sqrt{\lambda_2}, \ \lambda_3 = \lambda_3'/\sqrt{\lambda_2}.$$

Since we already know the critical stretches for creases under generalized plane strain condition (Fig. 6(c)), the critical strains for creases in plane strain condition can be calculated as $\lambda_1' = \lambda_1\sqrt{\lambda_2}$, where $\lambda_1 = 1 + e_{yy}$ and $\lambda_2 = 1 + e_{xx}$. The results show that the critical strains of creases increase with hysteresis (Fig. 6(e)). The critical strains with alginate/AAM = 0 and 2.78 wt% are around 0.35, which agrees with the reported value of crease formed in materials without hysteresis. The critical strains with alginate/AAM = 7.4 wt% and 16.72 wt% are higher than 0.35, which are 0.4 and 0.49, respectively. Even higher alginate concentration would lead to even higher critical strain, but is difficult to determine from our experiment setup.

That inelasticity affects the onset of creases can potentially enable the design of crease-resistant materials. Such crease-resistant materials may find applications in engineering, such as an adaptive lens that functions under various geometry and swelling state, a soft actuator that bends without creases, and a tire sustains large bending deformation without forming creases can prevent earlier failure. Because inelasticity is undesirable in many applications, a crease-resistant material should be designed such that it is elastic when stretch is modest, but becomes inelastic when stretch is large. Thus, in application, most part of the material is elastic, but the sites of stress concentration will undergo inelastic deformation and retard the onset of creases.

4. Conclusion

We use alg-PAAM hydrogels to study the effect of inelasticity on the onset of creases. We vary the alginate concentration in the alg-PAAM hydrogel to change its degree of inelasticity. A higher alginate concentration leads to a larger hysteresis, and also a larger energy dissipation. We conduct compression tests on disk-shape alg-PAAM hydrogels of varied alginate concentration, and show that creases form at a higher critical strain with higher alginate concentration. We further convert the critical strains measured in the experiment to those in plane strain condition, and show that the larger energy dissipation increases the critical strain for the onset of creases. Chemistry affects rheology, and rheology affects the onset of creases.

Declaration of competing interest

The authors declare that they have no known competing financial interests or personal relationships that could have appeared to influence the work reported in this paper.

Acknowledgments

References

[1] E. Hohlfeld, L. Mahadevan, Unfolding the Sulcus, Phys. Rev. Lett. 106 (10) (2011).

[2] E. Hohlfeld, L. Mahadevan, The sacle and nature of sulcification patterns, Phys. Rev. Lett. (2012) 109.

[3] A.N. Gent, I.S. Cho, Surface instabilities in compressed or bent rubber blocks, Rubber Chem. Technol. 72 (2) (1999) 253–262.

[4] W. Hong, X. Zhao, Z. Suo, Formation of creases on the surfaces of elastomers and gels, Appl. Phys. Lett. 95 (11) (2009).

[5] B. Li, et al., Mechanics of morphological instabilities and surface wrinkling in soft materials: a review, Soft Matter 8 (21) (2012) 5728–5745.

[6] A. Ghatak, A.L. Das, Kink instability of a highly deformable elastic cylinder, Phys. Rev. Lett. 99 (7) (2007).

[7] S. Mora, et al., Surface instability of soft solids under strain, Soft Matter 7 (22) (2011) 10612–10619.

[8] S. Cai, et al., Creasing instability of elastomer films, Soft Matter 8 (5) (2012) 1301–1304.

[9] T. Tanaka, et al., Mechanical Instability of Gels at the Phase-Transition, Nature 325 (6107) (1987) 796–798.

[10] V. Trujillo, J. Kim, R.C. Hayward, Creasing instability of surface-attached hydrogels, Soft Matter 4 (3) (2008) 564–569.

[11] K. Saha, et al., Surface creasing instability of Soft Polyacrylamide Cell Culture substrates, Biophys. J. 99 (12) (2010) L94–L96.

[12] J. Yoon, J. Kim, R.C. Hayward, Nucleation, growth, and hysteresis of surface creases on swelled polymer gels, Soft Matter 6 (22) (2010) 5807–5816.

[13] W. Barros, E.N. de Azevedo, M. Engelsberg, Surface pattern formation in a swelling gel, Soft Matter 8 (32) (2012) 8511–8516.

[14] F. Weiss, et al., Creases and Wrinkles on the Surface of a Swollen Gel, J. Appl. Phys. 114 (7) (2013) 073507.

[15] D.P. Richman, et al., Mechanical mode of brain convolutional development, Science 189 (1975) 18–21.

[16] J. Dervaux, et al., Shape transition in artificial tumors: from smooth buckles to singular creases, Phys. Rev. Lett. 107 (1) (2011) 018103.

[17] L. Jin, S. Cai, Z. Suo, Creases in soft tissues generated by growth, Epl 95 (6) (2011).

[18] T. Tallinen, et al., On the growth and form of cortical convolutions, Nat. Phys. (2016).

[19] B. Xu, R.C. Hayward, Low-Voltage Switching of crease Patterns on Hydrogel Surfaces, Adv. Mater. 25 (39) (2013) 5555–5559.

[20] Q. Wang, X. Zhao, Creasing-wrinkling transition in elastomer films under electric fields, Phys. Rev. E 88 (4) (2013) 042403.

[21] Q. Wang, L. Zhang, X. Zhao, Creasing to Cratering Instability in Polymers under Ultrahigh Electric Fields, Phys. Rev. Lett. 106 (11) (2011).

[22] Q. Wang, et al., Dynamic electrostatic Lithography: Multiscale on-demand Patterning on Large-Area Curved surfaces, Adv. Mater. 24 (15) (2012) 1947–1951.

[23] B. Xu, D. Chen, R.C. Hayward, Mechanically gated electrical switches by creasing of patterned Metal/Elastomer Bilayer Films, Adv. Mater. 26 (25) (2014) 4381–4385.

[24] N. Zalachas, et al., Crease in a ring of a pH-sensitive hydrogel swelling under constraint, Int. J. Solids Struct. 50 (6) (2013) 920–927.

[25] D. Chen, G.H. McKinley, R.E. Cohen, Spontaneous wettability patterning via creasing instability, Proc. Natl. Acad. Sci. 113 (29) (2016) 8087–8092.

[26] J. Yoon, et al., Local switching of Chemical Patterns through Light-Triggered unfolding of creased Hydrogel Surfaces, Angew. Chem. Int. Edn 51 (29) (2012) 7146–7149.

[27] J. Kim, J. Yoon, R.C. Hayward, Dynamic display of biomolecular patterns through an elastic creasing instability of stimuli-responsive hydrogels, Nature Mater. 9 (2) (2010) 159–164.

[28] J. Yang, et al., Plasticity retards the formation of creases, J. Mech. Phys. Solids 123 (2019) 305–314.

[29] Y.-P. Cao, et al., Wrinkling and creasing of a compressed elastoplastic film resting on a soft substrate, Comput. Mater. Sci. 57 (2012) 111–117.

[30] Q. Wang, et al., Electromechanical instabilities of thermoplastics: Theory and in situ observation, Appl. Phys. Lett. 101 (14) (2012).

[31] Y. Tanaka, K. Fukao, Y. Miyamoto, Fracture energy of gels, Eur. Phys. J. E 3 (4) (2000) 395–401.

[32] X. Zhao, Multi-scale multi-mechanism design of tough hydrogels: building dissipation into stretchy networks, Soft Matter 10 (5) (2014) 672–687.

[33] D.C. Tuncaboylu, et al., Tough and self-healing hydrogels formed via hydrophobic interactions, Macromolecules 44 (12) (2011) 4997–5005.

[34] T.L. Sun, et al., Physical hydrogels composed of polyampholytes demonstrate high toughness and viscoelasticity, Nature Mater. 12 (10) (2013) 932.

[35] R. Bai, et al., Fatigue fracture of self-recovery hydrogels, ACS Macro Lett. 7 (3) (2018) 312–317.

[36] K. Haraguchi, T. Takehisa, S. Fan, Effects of clay content on the properties of nanocomposite hydrogels composed of poly (N-isopropylacrylamide) and clay, Macromolecules 35 (27) (2002) 10162–10171.

[37] J.P. Gong, et al., Double-network hydrogels with extremely high mechanical strength, Adv. Mater. 15 (14) (2003) 1155–1158.

[38] J.-Y. Sun, et al., Highly stretchable and tough hydrogels, Nature 489 (7414) (2012) 133–136.

[39] S. Lin, et al., Design of stiff, tough and stretchy hydrogel composites via nanoscale hybrid crosslinking and macroscale fiber reinforcement, Soft Matter 10 (38) (2014) 7519–7527.

[40] C.H. Yang, et al., Strengthening alginate/polyacrylamide hydrogels using various multivalent cations, ACS Appl. Mater. Interfaces 5 (21) (2013) 10418–10422.